Journal of Electron Microscopy **54(3)**: 287–291 (2005)
doi:10.1093/jmicro/dfi039

Electron energy-loss spectroscopy study of ZnO nanobelts

Yong Ding[1] and Zhong Lin Wang[1,2,*]

[1]School of Materials Science and Engineering, Georgia Institute of Technology, 771 Ferst Drive, N. W., Atlanta, GA 30332-0245, USA and [2]National Center for Nanoscience and Nanotechnology, Beijing 100080, China
*To whom correspondence should be addressed. E-mail: zhong.wang@mse.gatech.edu

Abstract Nanobelts of ZnO have well-defined shapes that are enclosed by {0001}, $\{01\bar{1}0\}$ and $\{2\bar{1}\bar{1}0\}$ facets. The nanobelts grow along $[01\bar{1}0]$ and $[2\bar{1}\bar{1}0]$ with large flat surfaces of $\pm(0001)$ and $\pm(01\bar{1}0)$, respectively. Electron energy-loss spectroscopy has been applied to study the electronic structure of ZnO nanobelts of different growth orientations. A plasmon peak observed at 13 eV is suggested to be the result of polar surface excitation. The energy-loss near-edge structure of the oxygen K and zinc L_3 edges acquired from the two types of nanobelts show clear orientation dependence, and they agree well to the calculated results.

Keywords electron energy-loss spectroscopy, plasmon, energy-loss near-edge structure, ZnO, nanobelt, polar surface

Received 20 December 2004, accepted 23 Feburary 2005, online 25 August 2005

Introduction

Research in 1-D nanomaterials has received a lot of attention owing to their potential applications in nanoscience and nanotechnology [1,2]. ZnO, for example, is a semiconductor with a large band-gap of 3.4 eV [3], which has applications in optics, optoelectronics, sensors and actuators. Recently, a wide range of nanostructures of ZnO has been synthesized, including nanobelts, nanotube, nanocomb, nanoring, nanohelix and nanocages [4,5], which are good candidates for nano-cantilevers [6], and piezoelectric sensors and resonators [7].

Structurally, the wurtzite-structured ZnO is non-centro symmetric, and its property is anisotropic as well. It will be very interesting to investigate the electronic structure of ZnO nanostructures of different growth orientation. However, the diversity and lower purity of the samples prohibit the application of the well-established techniques such as XPS, AES and UPS. Electron energy-loss spectroscopy (EELS) has a high spatial resolution and gives the possibility of investigating the electronic structure of a nanobelt and a nanotube [8,9]. By combining the crystallographic and chemical information provided by transmission electron microscopy, EELS may have certain advantages for the investigation of nano scale electronic structures, although its energy resolution is limited.

In this study, the electronic structure of ZnO nanobelts was investigated using EELS. The surface plasmon oscillation located at 13 eV may be owing to the existence of the large polar surfaces. The projected density of states (DOS), along *c*-axis and perpendicular to *c*-axis, have been revealed from the energy-loss near-edge structure (ELNES) of oxygen K and zinc L_3 edges, and they match well to the calculated results.

Methods

ZnO nanobelts were synthesized by a solid–vapor deposition process: the detail description on synthesis and the structure of the nanobelts can be found elsewhere [4]. For this study, the as-synthesized nanobelts of different structural characteristics were deposited on holey carbon grids. Energy-loss spectra were acquired at 200 kV using a cold field emission transmission electron microscope (TEM) (Hitachi HF2000) equipped with a Gatan 666 parallel detection electron-energy-loss spectrometer (PEELS). The EELS spectra were acquired in the imaging mode using a 3 mm EELS entrance aperture. The energy resolution of the equipment is ~0.90 eV at 0.05 eV per channel at full beam illumination and good detectable signal.

Dedicated to the memory of John M. Cowley.

Results and discussion

The crystal structure of the nanobelt has been analyzed previously [4,5]. For this study, we focus on two types of nanobelts: one growing along $[01\bar{1}0]$ with large $\pm(0001)$ polar surfaces and the other growing along $[2\bar{1}\bar{1}0]$ with large $\pm(01\bar{1}0)$ surfaces. The nanobelt in Fig. 1a grows along $[01\bar{1}0]$, its top/bottom surface being (0001) and side surface $(2\bar{1}\bar{1}0)$. This type of nanobelts is called the polar surface dominated nanobelts. The nanobelt shown in Fig. 1c grows along $[2\bar{1}\bar{1}0]$, with large $\pm(01\bar{1}0)$ surfaces. This type of nanobelts is referred to as the non-polar nanobelt. The surface normal directions of the two types nanobelts are [0001] and $[01\bar{1}0]$, which are ideal for investigating the anisotropic electronic structure of ZnO as determined by its crystal structure.

The thickness of the nanobelts was determined using the low-loss energy spectra in reference to the inelastic mean-free-path length (Λ) for ZnO determined previously [10]. If we take Λ as 161 nm, the thicknesses of our nanobelts are 40–80 nm. It is important to have $t/\Lambda < 1$ to ensure the reliability of the acquired data, where t is the specimen thickness. Fourier-log deconvolution was applied to remove the plural scattering in EELS spectra. The program used to perform the Fourier-log deconvolution can be found in the appendix B.2 in ref. [11].

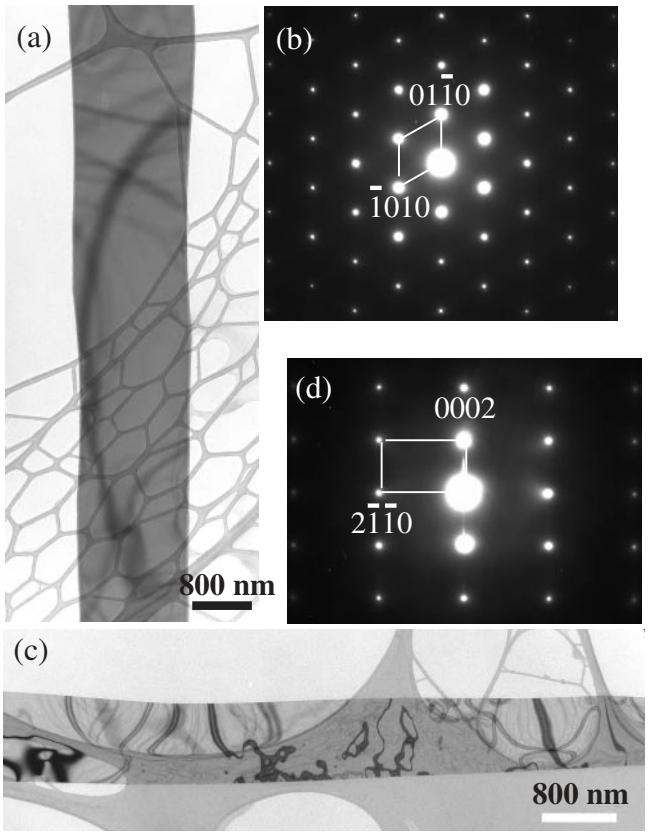

Fig. 1 (a and b) Bright-field image of ZnO nanobelt and its corresponding SAED pattern for a nanobelt that grows along $[01\bar{1}0]$ and is dominated by $\pm(0001)$ polar surface. (c and d) Bright-field image of ZnO nanobelt and its corresponding SAED pattern for a nanobelt that grows along $[2\bar{1}\bar{1}0]$ and is dominated by $\pm(01\bar{1}0)$ non-polar surface.

In EELS, the electronic structure of the sample is reflected by several inelastic interaction processes [11]. In the low-loss region, volume and surface plasma peaks are closely related to the dielectric response of the valence band. In higher energy-loss region, near-edge fine structure is related to the projected density of states in the conduction band. The following analysis is based on the information provided by plasmon and atomic inner shell excitations.

Surface energy-losses

We first focus on the low-loss energy spectra. Since ZnO is an anisotropic material, the dielectric functions parallel and perpendicular to the c-axis are different, $\varepsilon_{\perp}$ and $\varepsilon_{\parallel}$. The large collection angle of the EEL spectrometer in our experiments minimizes the difference contributed by momentum transfers in parallel and perpendicular cases to the electron beam [12]. Figure 2 shows a comparison of low-loss EELS spectra acquired from the two types of ZnO nanobelts. The incident electron beam was adjusted perpendicular to the large surface of the ZnO nanobelts, thus, from the crystallographic point of view, the spectra acquired from the two types of ZnO nanobelts correspond to electron beams parallel and perpendicular to the c-axis, respectively. The volume plasmon peak I_{P1} at 18.70 eV and surface plasmon peaks S_1 and S_2 at 9.45 and 13.00 eV agree to the observation by Hengehold *et al.* [13] using low-energy incident electrons with the beam closely parallel to the c-axis. The asymmetry of the I_{P1} is due to the existence of the S_3 peak. An interesting phenomenon is that the surface plasmon peak at 13.00 eV smears out when the spectra were acquired from the $[2\bar{1}\bar{1}0]$ growth nanobelts with the electron beam perpendicular to c-axis, as displayed in Fig. 2a. The spectrum in Fig. 2b is derived from the spectrum shown in Fig. 2a after applying the Fourier-log deconvolution to remove the multiple scattering effect [11]. After aligning the two spectra at the I_{P1} peak, they match very well except at the S_2 peak. Considering the anisotropic structure of ZnO, the S_2 peak might be the result of anisotropic excitation between the perpendicular and parallel to c-axis cases. But it could also be associated with the polar surface.

The structure of ZnO can be described as a number of alternating planes composed of tetrahedrally coordinated O^{2-} and Zn^{2+} ions, stacked alternatively along the c-axis. The oppositely charged ions produce positively charged Zn-(0001) and negatively charged O-$(000\bar{1})$ polar surfaces, resulting in a normal dipole moment and spontaneous polarization along the c-axis. If the elastic deformation energy is largely suppressed by reducing the thickness of a nanobelt, the polar-nanobelt could self-assemble into different shapes as driven by minimizing the electrostatic energy coming from the ionic charges on the polar surfaces [14]. The $[01\bar{1}0]$ growth nanobelt is dominated by the $\pm(0001)$ polar surfaces, while the $[2\bar{1}\bar{1}0]$ growth nanobelt is

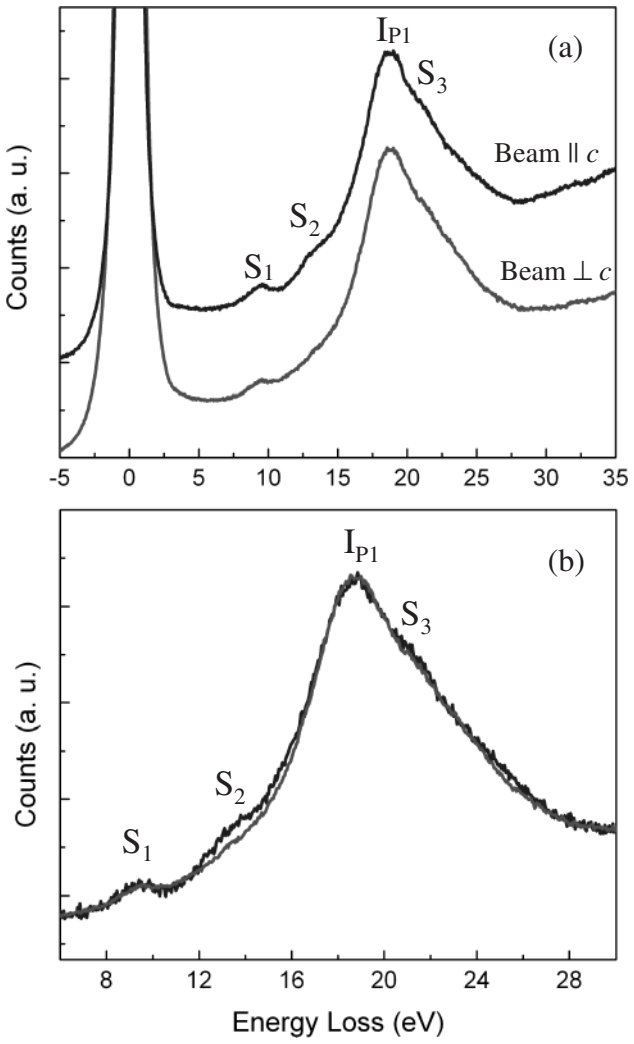

Fig. 2 (a) Low-loss energy spectra of the two types of nanobelts: polar surface dominant and non-polar dominant nanobelts, corresponding to the electron beam parallel and perpendicular to *c*-axis. (b) The EELS spectra shown in (a) after being processed by the Fourier-log deconvolution for removing multiple scattering.

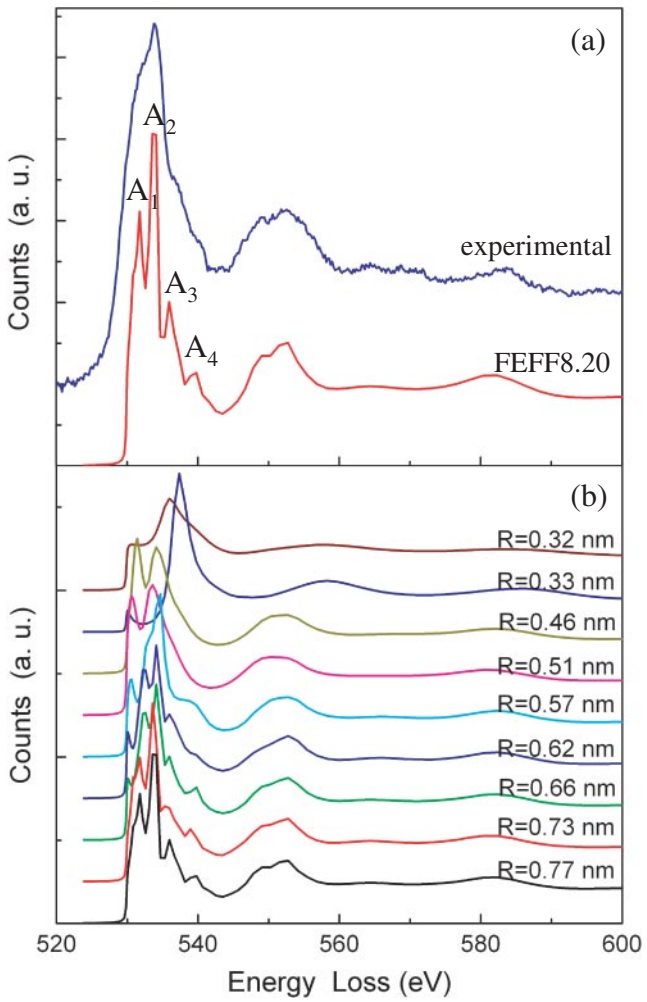

Fig. 3 (a) Experimental and simulated oxygen K-edge ELNES spectra for a non-polar nanobelt. (b) Simulated spectra using the FEFF8.20 program by changing the radius of the ZnO cluster.

dominated by the non-polar $\pm(01\bar{1}0)$ surfaces. The fact is that the S_2 peak shows up only in the spectra acquired from the polar surface dominated nanobelts. It is thus suggested that the S_2 peak at 13 eV could be closely related to the electronic structure of the $\pm(0001)$ polar surfaces.

Oxygen K-edge ionization

In the higher energy-loss region, the observable ionization edges are O-K and Zn-L. Figure 3a shows the Fourier-ratio deconvoluted [11] experimental and the simulated oxygen K-edge ELNES of ZnO nanobelts with electron beam closely parallel to the *c*-axis of ZnO. The simulation was carried out using the FEFF8.20 commercial program [15], developed for simulating the X-ray absorption near-edge structure (XANES). Although the ELNES and XANES use different excitation sources, they both provide information about the local electronic structure. The results presented in Fig. 3a show good agreement between the experimental spectrum and the calculated one taking into account the limited energy resolution in the experiments.

The ELNES is strongly affected by the scattering at the vicinity of the probed atom; the calculated result can provide the effective radius of interaction for explaining the observed ELNES. The simulated spectra obtained by changing the size of the ZnO cluster are shown in Fig. 3b. The effective radius required for the calculation to converge can be estimated by comparison with the experimental spectrum, and the result is $R \sim 0.73$ nm. This parameter is thus adopted for all of the calculations to be presented in the following sections.

The anisotropic electronic structure of ZnO can be seen through the EELS. To detect the electronic structure with the beam parallel to the *c*-axis, the ***E*** polarization direction of X-ray should be perpendicular to *c*-axis. That is why the experimental data acquired with the electron beam parallel to the *c*-axis could be compared with the calculation made for polarization perpendicular to the *c*-axis. Figure 4a shows a comparison of the oxygen K-edge acquired from the two

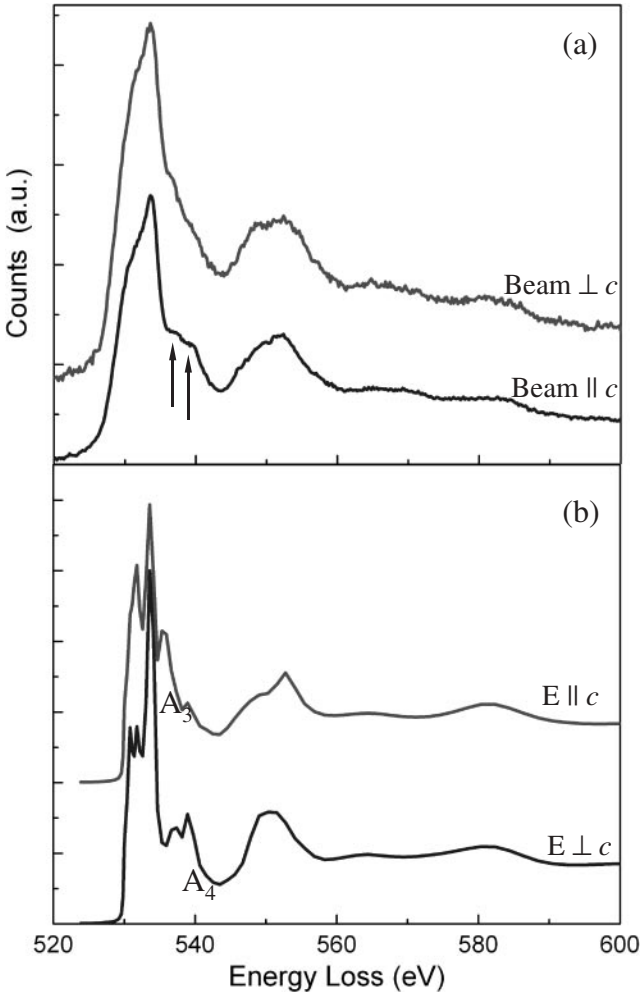

Fig. 4 (a) Experimental and (b) simulated EELS spectra of oxygen K-edge for the two types of nanobelts.

types of ZnO nanobelts: polar surface dominant and non-polar nanobelts corresponding to the incident beam parallel and perpendicular to the *c*-axis. The difference is significant, especially at the energies indicated by the arrowheads. Using the FEFF8.20 program, we have calculated the XANES for the two cases by adjusting the polarization direction ***E*** of the X-ray beam, and the results are presented in Fig. 4b. The distinct difference at peaks A_3 and A_4 is apparent, in agreement with the experimental data.

The ELNES of ZnO is sensitive to the orientation of the crystal. The spectra a, b and c given in Fig. 5 were acquired by tilting the [01$\bar{1}$0] growth ZnO nanobelts by 0°, 10° and 20° with respect to the *c*-axis. A change in the intensity of the A_4 peak is obvious. The spectrum c acquired at 20° from the *c*-axis is fairly close to the spectrum acquired when the beam is perpendicular to the *c*-axis (see Fig. 4a).

Zinc L-edge ionization

The zinc L-edge ELNES spectra acquired from [01$\bar{1}$0] and [2$\bar{1}\bar{1}$0] growth ZnO nanobelts are displayed in Fig. 6a. The L_1, L_2 and L_3 can be clearly identified. Only the L_3 edge at the

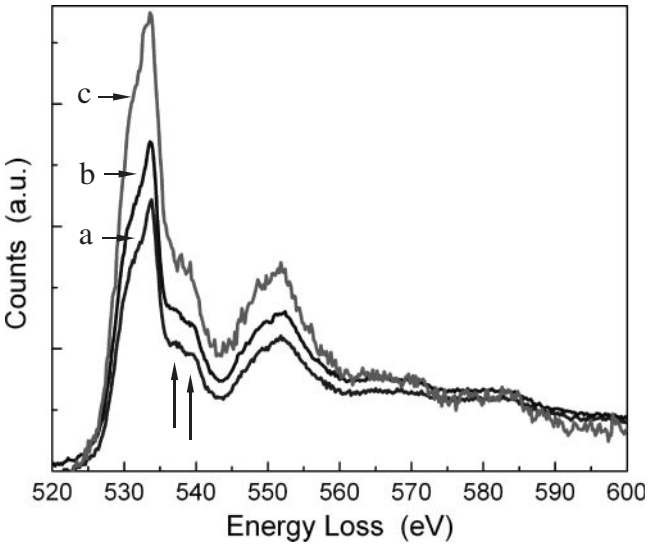

Fig. 5 Dependence of oxygen K-edge on the angle of the incident electron beam with the *c*-axis for a polar nanobelt: a: ∼0°; b: ∼10°; c: ∼20°.

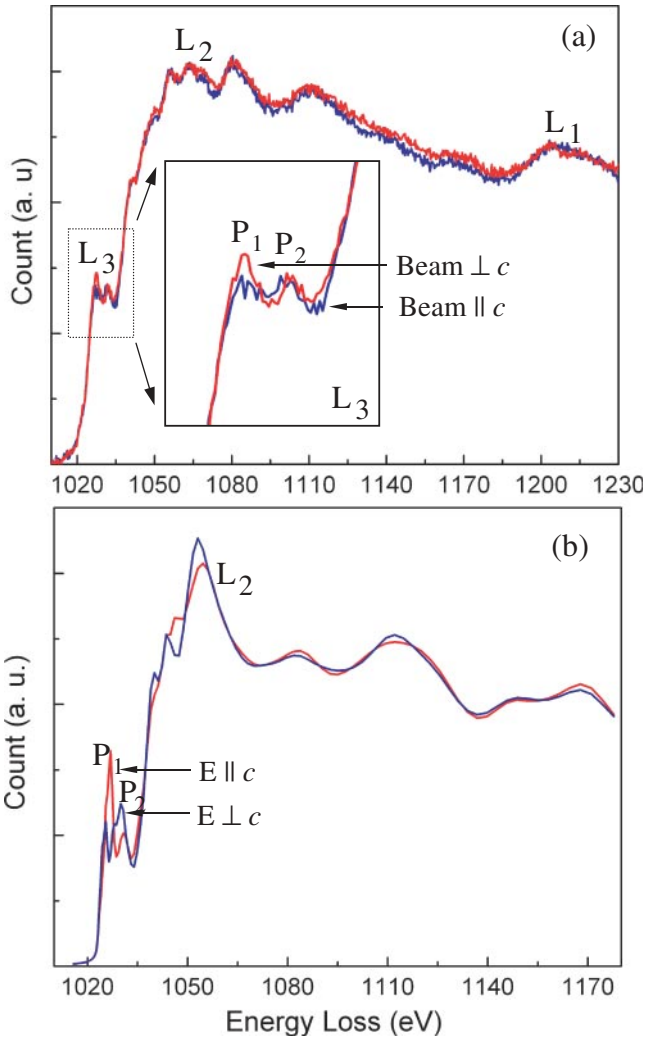

Fig. 6 (a) Experimental and (b) simulated EELS spectra of zinc L-edge for the two types of nanobelts.

edge threshold shows a difference. The L_3 edge is composed of two peaks: P_1 and P_2. When electron beam changes from parallel to perpendicular to *c*-axis, the intensity of P_1 shows a small jump. This result has been confirmed by the simulation using the FEFF8.20 program, as shown in Fig. 6b, by choosing the polar direction of the incident X-ray photon to be parallel and perpendicular to the *c*-axis. Mizoguchi *et al*. [16] gave a theoretical prediction about the anisotropy of the oxygen K-edge and Zn L_3 edge of ZnO. The results of their calculations are consistent with our experimental results as well as our calculations using the FEFF8.20 program.

Concluding remarks

EELS has been used to study the electronic structure of ZnO nanobelts. The polar surface dominant [01$\bar{1}$0] growth ZnO nanobelts show an extra surface plasmon peak at 13.0 eV compared with that from the non-polar surface dominant [2$\bar{1}\bar{1}$0] growth nanobelts, which is suggested to be related to the polar surface. Crystallographic orientation dependence on the ELNES of different types of nanobelts has been investigated. The observed fine structures at the oxygen K-edge and zinc L_3 edge agree with the calculated results.

Acknowledgements

This work is supported by NASA Vehicle Systems Program, and Department of Defense Research and Engineering (DDR&E) and DARPA.

References

1 Wang Z L, ed. (2003) *Nanowires and Nanobelts, Vol. I: Metal and Semiconductor, Nanowires*. (Kluwer Academic Publisher, New York).

2 Wang, Z L, ed. (2003) *Nanowires and Nanobelts, Vol. II: Nanowires and Nanobelts of Functional Materials*. (Kluwer Academic Publisher, New York).

3 Srikant V and Clarke D R (1998) On the optical band gap of zinc oxide. *J. Appl. Phys.* **83**: 5447–5451.

4 Pan Z W, Dai Z R, and Wang Z L (2001) Nanobelts of semiconducting oxides. *Science* **291**: 1974–1979.

5 Kong X Y and Wang Z L (2003) Spontaneous polarization-induced nanohelixes, nanosprings, and nanorings of piezoelectric nanobelts. *Nano Lett.* **3**: 1625–1631.

6 Hughes W L and Wang Z L (2002) Nanobelts as nanocantilevers. *Appl. Phys. Lett.* **82**: 2886–2888.

7 Comini E, Faglia G, Sberveglieri G, Pan Z W, and Wang Z L (2002) Stable and highly sensitive gas sensors based on semiconducting oxide nanobelts. *Appl. Phys. Lett.* **81**: 1869–1871.

8 Stöckli T, Bonard J-M, Châtelain A, Wang Z L, and Stadelmann P (2002) Valence excitations in individual single-walled carbon nanotubes. *Appl. Phys. Lett.* **80**: 2982–2984.

9 Stöckli T, Wang Z L, Bonard J-M, Stadelmann P, and Châtelain A (1999) Plasmon excitation in carbon nanotubes. *Phil. Mag. B* **79**: 1531–1548.

10 Berta Y, Ma C, and Wang Z L (2002) Measuring the aspect ratios of ZnO nanobelts. *Micron* **33**: 687–691.

11 Egerton R F (1996) *Electron Energy-Loss Spectroscopy in the Electron Microscope*, 2nd edn. (Plenum Press, New York and London).

12 Zhu Y, Wang Z L, and Suenaga M (1993) Grain boundary studies by the coincidence site lattice model and electron energy loss spectroscopy of the oxygen K-edge in $YBa_2Cu_3O_7$-X. *Phil. Mag. A* **67**: 11–28.

13 Hengehold R H, Almassy R J, and Pedrotti F L (1970) Electron energy-loss and ultraviolet-reflectivity spectra of crystalline ZnO. *Phys. Rev. B* **1**: 4784–4791.

14 Wang Z L, Kong X Y, Ding Y, Gao P X, Hughes W L, Yang R S, and Zhang Y (2004) Semiconducting and piezoelectric oxide nanostructures induced by polar surfaces. *Adv. Funct. Mater.* **14**: 944–956.

15 Ankudinov A L, Bouldin C, Rehr J J, Sims J, and Hung H (2002) Parallel calculation of electron multiple scattering using Lanczos algorithms. *Phys. Rev. B* **65**: 104107–104118.

16 Mizoguchi T, Tanaka I, Yoshioka S, Kunisu M, Yamamoto T, and Ching W Y (2004) First-principles calculations of ELNES and XANES of selected wide-gap materials: dependence on crystal structure and orientation. *Phys. Rev. B* **70**: 045103-1–045103-10.